



# Common mechanism for inter-annual and decadal variability in the East African long rains

Dean P. Walker<sup>1</sup>, John H. Marsham<sup>1,2</sup>, Cathryn E. Birch<sup>1</sup>, Adam A. Scaife<sup>3,4</sup>,  
Declan L. Finney<sup>1</sup>

<sup>1</sup>School of Earth and Environment, University of Leeds, Leeds, UK

<sup>2</sup>National Centre for Atmospheric Science, Leeds, UK

<sup>3</sup>Met Office Hadley Centre, Exeter, UK

<sup>4</sup>College of Engineering, Mathematics and Physical Sciences, University of Exeter, Exeter, UK

## Key Points:

- East African long rains inter-annual and decadal variability have the same quantitative link to winds across the Congo and Gulf of Guinea
- Drier long rains and the corresponding zonal wind anomalies are linked to Sahelian warming on both inter-annual and decadal timescales
- The Madden-Julian Oscillation influences both the zonal winds and the long rains on inter-annual and decadal timescales

---

Corresponding author: Dean P. Walker, [eedpw@leeds.ac.uk](mailto:eedpw@leeds.ac.uk)

This article has been accepted for publication and undergone full peer review but has not been through the copyediting, typesetting, pagination and proofreading process which may lead to differences between this version and the Version of Record. Please cite this article as doi: 10.1029/2020GL089182

**Abstract**

The East African long rains constitute the main crop-growing season in the region. Inter-annual predictability of this season is low in comparison to the short rains, and recent decadal drying contrasts with climate projections of a wetter future (the “East African climate paradox”). Here, we show that long rains rainfall totals are strongly correlated with 700hPa zonal winds across the Congo basin and Gulf of Guinea ( $r=0.73$ ). Westerly anomalies align with more rainfall, with the same mechanism controlling co-variability on inter-annual and decadal timescales. On both timescales wind anomalies are linked to geopotential anomalies over the Sahel and Sahara, and warming there. Rainfall and wind are significantly correlated with the Madden-Julian Oscillation (MJO) amplitude, and around 18% of the decadal drying can be explained by MJO amplitude variability. This work shows that predictions of East African rainfall across timescales require robust prediction of both zonal winds and MJO activity.

**Plain Language Summary**

East Africa has two rainfall seasons, the main season, the long rains, runs from March to May. There is currently little understanding of what controls the amount of rainfall during this season. Recent drying, causing many areas to suffer from droughts and food shortages, contrasts with climate projections of a wetter future (the “East African climate paradox”). Rainfall is found to be connected to the strength of easterly winds over the Congo basin and Gulf of Guinea, with the same mechanism controlling variability on both inter-annual and decadal timescales. From 1998 to 2011 the winds had been getting stronger, with reduced rainfall over East Africa. The cause of the stronger wind is investigated, and is partly explained by relatively faster warming in the Sahel than over the Congo, whilst variation in Madden-Julian Oscillation (a large scale tropical wave) activity, explains around 18% of the decadal drying.

**1 Introduction**

Equatorial East Africa has two rainfall seasons per year, the long rains, occurring March-May (MAM), and short rains, occurring October-December (OND). A large contrast in the predictability of the two seasons has been observed (Camberlin & Philippon, 2002; Batté & Déqué, 2011; Dutra et al., 2013; Nicholson, 2017; Walker et al., 2019). This

46 has been attributed to the short rains being influenced by global scale modes of variabil-  
47 ity such as El Niño-Southern Oscillation (Nicholson & Entekhabi, 1986; Indeje et al., 2000),  
48 and the Indian Ocean Dipole (Saji et al., 1999; Black et al., 2003), whilst such relation-  
49 ships are absent during the long rains (Ogallo, 1988).

50 In most areas of equatorial East Africa, the long rains is the main crop growing sea-  
51 son, generally providing greater (Camberlin & Wairoto, 1997), and more reliable (Camberlin  
52 & Philippon, 2002), rainfall amounts. However, in recent decades there has been an ob-  
53 served drying trend in this season (Funk et al., 2005, 2008; Liebmann et al., 2014; Maid-  
54 ment et al., 2015), which sharply contrasts the wetting predicted by most climate pro-  
55 jections (Shongwe et al., 2011; Otieno & Anyah, 2013), often referred to as the “East African  
56 Climate Paradox” (Rowell et al., 2015). Some authors have demonstrated that the long  
57 rains decline is linked with natural decadal variability in the Pacific Ocean (Lyon, 2014;  
58 Yang et al., 2014; Bahaga et al., 2019), whilst others suggest anthropogenic factors (Williams  
59 & Funk, 2011; Funk & Hoell, 2015; Rowell et al., 2015). Meanwhile, recent work by Wainwright  
60 et al. (2019) has shown that over the Horn of Africa the observed long rains drying trend  
61 is caused by a shortening of the rainfall season, and that in more recent years, the long  
62 rains have begun to recover. Therefore the future of the long rains is still highly uncer-  
63 tain. Improved understanding and prediction of variability in this season on inter-annual  
64 and decadal timescales, leading to improved rainfall forecasts, would be of great bene-  
65 fit to the local population.

66 Finney et al. (2019) recently demonstrated that although the climatological wind  
67 is easterly (Figure S1a), days with westerly winds originating from over the Congo basin  
68 do occur during the long rains season, and throughout the year. These events import  
69 moist air from over the Congo basin, causing convergence within the Lake Victoria basin,  
70 thereby leading to enhanced rainfall, with the record breaking 2018 long rains serving  
71 as a prime example (Kilavi et al., 2018). During MAM 2018 several westerly days oc-  
72 curred, linked to tropical cyclones in the Indian Ocean. Finney et al. (2019) also high-  
73 lighted the role of the Madden-Julian Oscillation (MJO; Madden & Julian, 1971, 1972)  
74 influencing the formation of these tropical cyclones.

75 A more direct effect of MJO influence on the long rains has been documented by  
76 Pohl and Camberlin (2006b, 2006a). Pohl and Camberlin (2006b), using phases of the  
77 MJO defined by Wheeler and Hendon (2004), identified that phases 2-3 from the Wheeler-

78 Hendon index, when the convective core is over Africa and the Indian Ocean, were linked  
79 to increased rainfall over the East African highlands. Meanwhile, Vellinga and Milton  
80 (2018) demonstrated that a greater seasonal mean amplitude of the MJO as defined by  
81 Wheeler and Hendon (2004), regardless of phase, contributed to more abundant rain-  
82 fall, due to an asymmetric response of the rainfall to the ascent/ descent caused by spe-  
83 cific phases.

84 Whilst anomalous westerly wind influence over East Africa has been regularly de-  
85 scribed qualitatively in past literature (Camberlin & Wairoto, 1997; Okoola, 1999a, 1999b;  
86 Diem et al., 2019; Nkunzimana et al., 2019), little quantitative evidence for this had been  
87 presented until the work by Finney et al. (2019). Finney et al. (2019) showed the role  
88 of absolute westerlies for East African rainfall; this work uses this understanding to demon-  
89 strate the connection between zonal wind anomalies and East African rainfall on both  
90 inter-annual and decadal timescales, demonstrating a link between long term change in  
91 the zonal winds over the Congo basin and the long rains drying trend (Section 3.1), and  
92 also investigating explanations for variability of the zonal winds (Section 3.2).

## 93 **2 Data and Methods**

94 The rainfall data for this study are Global Precipitation Climatology Project Ver-  
95 sion 2.3 (GPCP; Adler et al., 2003), whilst wind, geopotential height, and temperature  
96 data were obtained from European Centre for Medium-Range Weather Forecasts (ECMWF)  
97 Interim Reanalysis (ERA-Interim; Dee et al., 2011). MJO phase and amplitude data were  
98 obtained from the Bureau of Meteorology, where phase and amplitude are calculated us-  
99 ing the method outlined in Wheeler and Hendon (2004), using National Oceanic and At-  
100 mospheric Administration (NOAA) outgoing long-wave radiation satellite observations  
101 (Liebmann & Smith, 1996), and National Centers for Environmental Prediction-National  
102 Centre for Atmospheric Research (NCEP-NCAR; Kalnay et al., 1996) reanalysis winds.  
103 National Aeronautics and Space Administration (NASA) Modern Era Retrospective Anal-  
104 ysis for Research and Applications, Version 2 (MERRA-2; Gelaro et al., 2017) winds and  
105 geopotential height data were used to verify relations between ERA-Interim variables  
106 and other observations.

107 This study uses the period 1979-2018, matching the satellite era and earliest avail-  
108 able data from ERA-Interim and GPCP. Results were tested with the outlying year 2018

109 removed, with similar conclusions. The region considered for rainfall is highlighted in  
 110 blue in Figure 1a, and future references to East Africa will refer to this region, whilst  
 111 the zonal wind index is calculated as the mean 700hPa zonal wind within 5°N to 5°S,  
 112 10°W to 30°E (brown box on Figure 1d,e).

113 Wet, dry, and recovery periods of the long rains, similar to those in Wainwright et  
 114 al. (2019), are defined from 1979-1997 (P1), 1998-2011 (P2), and 2012-2018 (P3) respec-  
 115 tively. Composites of the drying trend are considered using P2–P1. The wettest and dri-  
 116 est years are calculated by fitting a cubic polynomial to the raw time series data, and  
 117 then removing this, to remove long term trends. The wettest and driest years within the  
 118 long rains are defined as years where the rainfall total after trend removal is more than  
 119 0.8 standard deviations above and below the 1979-2018 seasonal mean respectively. When  
 120 discussing these sets of years, DECADEAL will refer to the altered Wainwright periods  
 121 (P2–P1), and INTERANNUAL will refer to the driest minus wettest years. Significance  
 122 of trends were tested using the Mann-Kendall test, (Mann, 1945; Kendall, 1975), further  
 123 details of which can be found in Wilks (2011).

124 The expected trend in mean rainfall between P1 and P2,  $\Delta\bar{r}_{exp}$ , due to the observed  
 125 change in mean wind from P1 to P2,  $\bar{u}_{P2} - \bar{u}_{P1}$ , is given by:

$$126 \quad \Delta\bar{r}_{exp} = \frac{dr}{du}(\bar{u}_{P2} - \bar{u}_{P1}) \quad (1)$$

127 where  $\frac{dr}{du}$  is the gradient of the regression of rainfall against wind after removing the poly-  
 128 nomial fit. Variables  $r$  and  $u$  can be replaced by other variables. If  $\Delta\bar{r}_{exp} \approx \Delta\bar{r}_{obs}$ , where  
 129  $\Delta\bar{r}_{obs}$  is the observed change in rainfall, then this is evidence that the mechanism that  
 130 links rainfall and winds on inter-annual timescales can also explain the decadal variabil-  
 131 ity in the rainfall.

### 132 **3 Results**

#### 133 **3.1 Inter-annual and decadal variability of the long rains**

134 Figure 1 shows rainfall anomalies over the tropics and 700hPa wind anomaly com-  
 135 posites over Africa for INTERANNUAL and DECADEAL. The 700hPa level was chosen  
 136 as it is largely above the topography of East Africa, and was found to have the largest  
 137 single level moisture flux, and moisture flux anomaly in the INTERANNUAL compos-  
 138 ite (Figure S1b). In Figure 1b,c a dry signal is apparent over East Africa as expected,

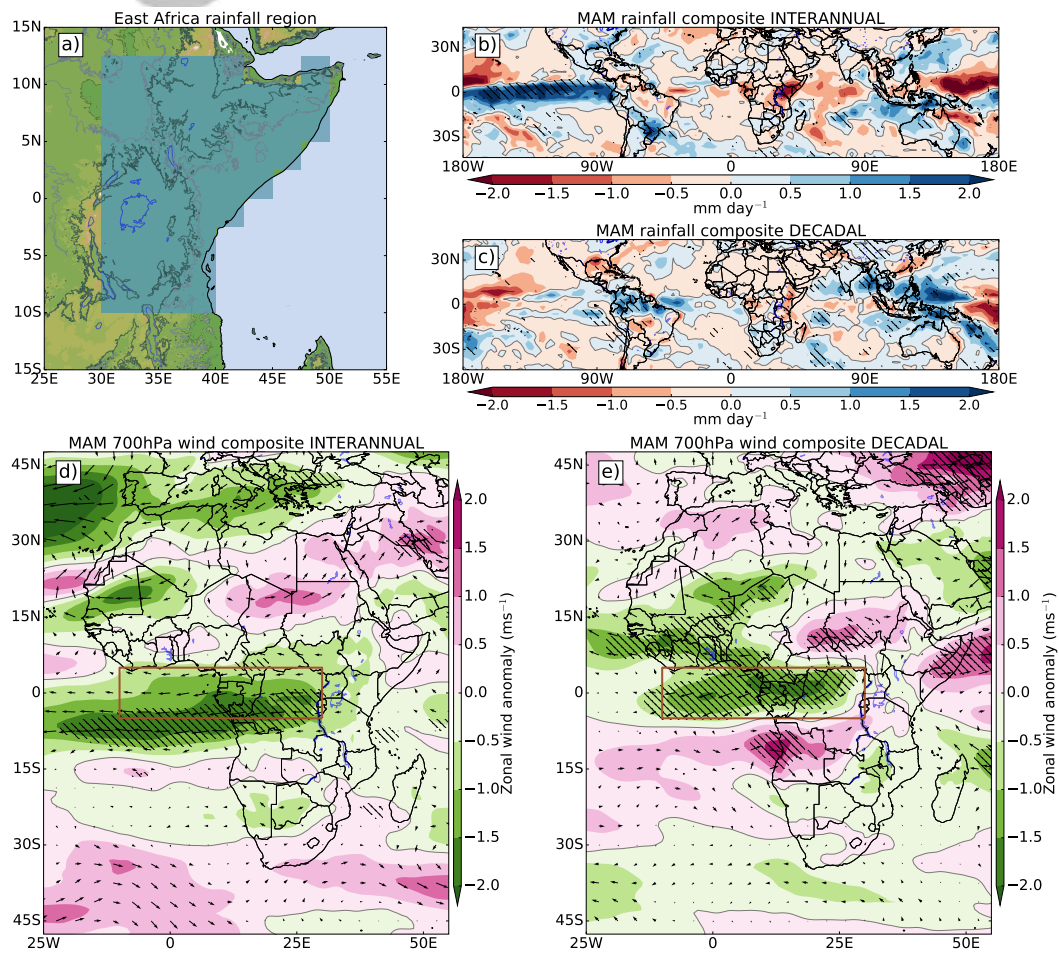


**Figure 1.** Inter-annual and decadal rainfall changes in East Africa. (a) East Africa rainfall region shaded blue (land within 10°N to 15°S, 30°E to 52.5°E), East Africa topography, colours, 500m and 1000m contours in light and dark grey. Composite of rainfall across the tropics during the long rains for (b) Driest years minus wettest years, (c) dry period minus wet period (P2–P1). Composite of 700hPa winds and zonal wind (colours) across Africa during the long rains for (d) Driest years minus wettest years, (e) Dry period minus wet period (P2–P1). Brown boxes show region used to calculate zonal wind index, hatching denotes areas where the composite values are significantly different from 0.

139 with wet anomalies over the Maritime Continent, and dry anomalies over the western  
140 Pacific, in a pattern reminiscent of the Pacific ‘V’ discussed in Lyon and Dewitt (2012);  
141 Funk and Hoell (2015); Funk et al. (2019). In Figure 1d,e a large easterly anomaly is present  
142 over the equatorial Atlantic Ocean and Congo basin. In INTERANNUAL, this extends  
143 to the Horn of Africa where it meets a westerly anomaly from the Indian Ocean, whilst  
144 in DECADEAL this easterly anomaly is also present, but only reaches as far as the orog-  
145 raphy separating the Congo basin from East Africa. In DECADEAL, the easterly anoma-  
146 lies appear to be linked to an anticyclonic anomaly over the Sahara desert; this level ex-  
147 hibits a mid-tropospheric high pressure, over the location of the summertime Saharan  
148 Heat Low (SHL), suggesting a stronger SHL in drier years (Evan et al., 2015). Heating  
149 and ascent in the SHL causes a low pressure near the surface and high pressure aloft at  
150 700hPa (Rácz & Smith, 1999; Lavaysse et al., 2009) and the 925 to 700hPa thickness is  
151 directly proportional to the air temperature in the column. The 700hPa anticyclone is  
152 therefore a useful measure of the SHL. The zonal wind anomaly (outlined by the brown  
153 box) is largely consistent with the findings of Finney et al. (2019), as an easterly anomaly  
154 in the seasonal mean is likely to contain less westerly, or weak easterly days. These re-  
155 sults are insensitive to the reanalysis used, with similar patterns observed in equivalent  
156 MERRA-2 composites (Figure S2a,b).

157 Figure 2 shows the time series of the zonal wind index, and long rains seasonal rain-  
158 fall anomalies. A correlation between the rainfall and zonal winds of 0.73 is found, 0.67  
159 with polynomial fits removed (both significant at the 1% level). This demonstrates the  
160 very strong connection between inter-annual variability in zonal wind and rainfall. This  
161 is again consistent in MERRA-2, with correlations of 0.81 (0.71 when detrended; Fig-  
162 ure S2c). It is apparent from Figure 2a that both the rainfall and zonal wind demon-  
163 strate a decreasing trend, both significant at the 5% level, when treated linearly, using  
164 the Mann-Kendall trend test. Both variables show some signs of a recovery in P3, con-  
165 sistent with Wainwright et al. (2019). This is more apparent in the rainfall than winds  
166 in Figure 2a, whilst for MERRA-2 (Figure S2c) a recovery in the zonal winds is more  
167 visible.

168 Figure 2b shows the scatter of rainfall against zonal wind after detrending. The  
169 linear regression equation between the two variables is  $r = 0.43u - 0.00$ . From this,  
170 and from the linear trend of each variable, an expected trend of rainfall due to the ob-  
171 served trend in the zonal winds can be calculated (Equation 1). The expected change

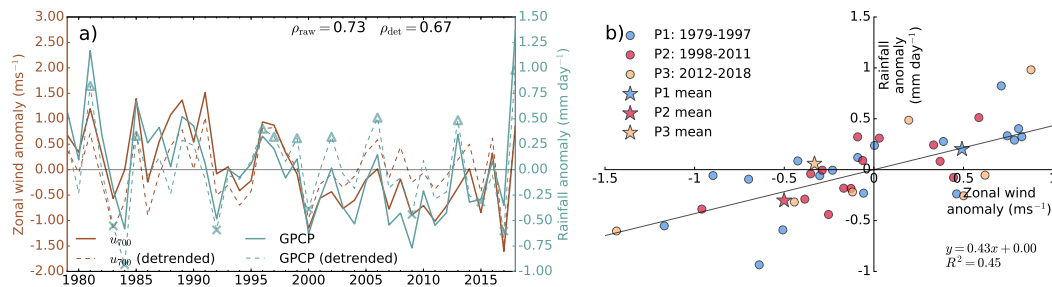


**Figure 2.** Temporal variations in East African rainfall and winds. (a) Time series of seasonal mean zonal wind anomaly (brown) and rainfall anomaly (blue) for boxes defined in Figure 1, dashed lines show time series after removing polynomial fit. The wet and dry years used for the INTERANNUAL composites are highlighted as triangles and crosses respectively. Correlation values of zonal winds against rainfall, before and after detrending given in top right. (b) Scatter of zonal wind anomaly against rainfall anomaly after detrending, coloured by P1 (blue), P2 (red), and P3 (yellow) periods. Black line is regression line fitted against the scatter, with regression equation and  $R^2$  value given. Coloured stars show mean anomaly of each period, with respect to 1979-2018 mean, before trend is removed.

172 in mean rainfall from observed change in mean zonal wind from P1 to P2 is  $-0.43 \pm 0.14$   
 173  $\text{mm day}^{-1}$ , the observed change is  $-0.50 \pm 0.16 \text{ mm day}^{-1}$ . These are statistically indis-  
 174 tinguishable, so it is concluded that the observed decadal drying in the long rains can  
 175 be largely explained by the same mechanism controlling the inter-annual relation between  
 176 the zonal wind and rainfall.

177 Whilst it is difficult to establish causality between the variability in the zonal winds  
 178 and rainfall, and is likely the two operate in a coupled system, (Finney et al., 2019) pro-  
 179 vides a potential mechanism. By examining lagged relationships it is found that zonal  
 180 winds early in the long rains (March) are more strongly correlated with rainfall later in  
 181 the season (April-May), than the inverse (0.61 compared to 0.37). By also considering  
 182 daily zonal winds against rainfall, it is found that the peak correlation occurs at 1 day  
 183 lag (zonal wind of one day against rainfall of the next), and is found to be significantly  
 184 higher than a 1 day lead correlation. Therefore both monthly and daily analysis support  
 185 wind anomalies leading to rainfall anomalies.

### 186 3.2 Drivers of variability of the zonal winds

187 As the main conclusion of Section 3.1 is that the zonal winds are strongly corre-  
 188 lated with the long rains on the inter-annual timescale, and can explain the decadal dry-  
 189 ing trend, an important question is to understand what is controlling variability in these  
 190 zonal winds on inter-annual and decadal timescales.

191 Recent work has shown the influence of the MJO amplitude on the long rains on  
 192 inter-annual timescales (Pohl & Camberlin, 2006a; Vellinga & Milton, 2018). Figure 3a  
 193 shows the time series of rainfall and zonal wind index alongside the February-March MJO  
 194 amplitude used in Vellinga and Milton (2018). Correlation between MJO amplitude and  
 195 zonal winds is 0.31, and between MJO and rainfall is 0.36 (0.34 and 0.35 respectively when  
 196 detrended). These fairly weak correlations are nevertheless significant at the 5% level,  
 197 and correlations between MJO and zonal wind are stronger in MERRA-2 (0.48, 0.54 when  
 198 detrended). In Figure 3a, there is significantly lower (at 5% level) mean MJO amplitude  
 199 during P2 than P1 and P3. The mean MJO amplitude of P2 is  $1.31 \pm 0.07$  whilst P1 and  
 200 P3 are  $1.53 \pm 0.11$  and  $1.70 \pm 0.09$  respectively. The zonal wind index was regressed against  
 201 the MJO amplitude ( $a$ ), giving a regression equation of  $u = 0.58a - 0.86$ . The change  
 202 in mean MJO amplitude from P1 to P2 is  $-0.21 \pm 0.14$ , giving an expected change in mean  
 203 zonal wind of  $-0.13 \pm 0.07 \text{ms}^{-1}$  from Equation 1. The observed change in the zonal wind  
 204 from P1 to P2 is  $-0.99 \pm 0.26 \text{ms}^{-1}$ , meaning approximately 13% of the change in zonal  
 205 wind can be attributed to the decrease in MJO amplitude. Similarly, regressing the rain-  
 206 fall against the MJO amplitude leads to an expected change of  $-0.09 \pm 0.10 \text{mm day}^{-1}$ .  
 207 The observed change in mean of the rainfall from P1 to P2 is  $-0.50 \pm 0.14 \text{mm day}^{-1}$ ,  
 208 so approximately 18% of the change in rainfall can be attributed to the decrease in MJO  
 209 amplitude.

210 Pohl and Camberlin (2006b) highlighted how different phases of the MJO influence  
 211 winds around East Africa, some phases giving easterly anomalies, others westerly, so it  
 212 is likely that by considering only amplitude these opposite influences mostly cancel out,  
 213 accounting for the low correlations when amplitude alone is considered. However, if the  
 214 wind response to phases is asymmetric, as for rainfall (Vellinga & Milton, 2018), this could  
 215 explain the significant correlation, providing evidence that the MJO influences inter-annual  
 216 and decadal variability of the zonal winds. Alternatively it may be that the mechanism  
 217 driving variability in the zonal winds also impacts MJO amplitude. The effects of dif-

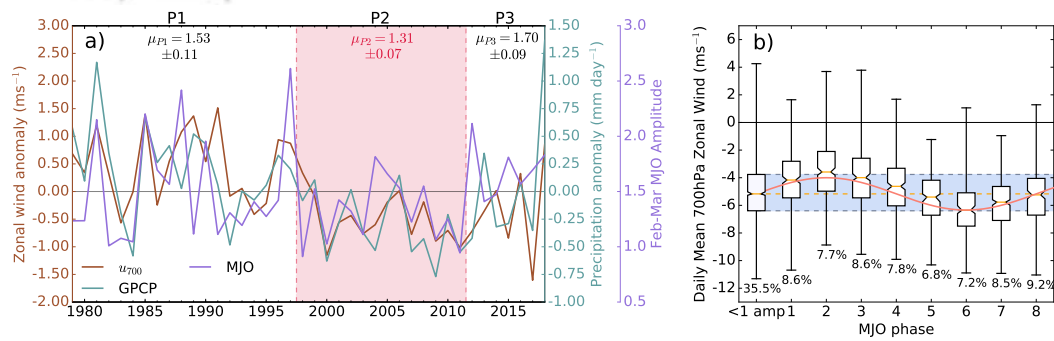


**Figure 3.** The MJO and East African rainfall. (a) Time series of zonal wind anomaly (brown) and rainfall anomaly (blue) as in Figure 2a, and February-March mean MJO amplitude (purple), means and standard errors of the MJO amplitudes during P1, P2, and P3 are given at the top, with periods separated by red dashed lines, and red shading over the dry period, P2. (b) Box plots of daily mean zonal wind separated by MJO phase, inactive days (MJO amplitude < 1) grouped in left box, notches on boxes show 95% confidence interval calculated from bootstrap resampling of 1000 values, numbers below min of each box show percentage of days in that phase, blue shading shows interquartile range of inactive days, orange dashed line shows median of inactive days. Pink curve shows sine wave fitted to active days assuming a mean value equal to the median of the inactive days.

218 ferent phases of the MJO on the zonal winds and rainfall are considered. Figure 3b shows  
219 box and whisker diagrams of the daily mean of the zonal wind index, separated by MJO  
220 phase, and separated into inactive days (amplitude  $< 1$ ) and active days (amplitude  $>$   
221  $1$ ), in MAM. If the zonal winds of the inactive days are more strongly easterly than the  
222 active days, it can be concluded that the influence of the MJO on wind is asymmetric  
223 as discussed above. To determine this, it is assumed that the converse is true: the mean  
224 winds of active and inactive days are the same. A sinusoidal wave is fitted based on this  
225 assumption, however, the wind is overall less easterly than predicted by the curve, im-  
226 plying that the mean winds of active and inactive days are different. In particular, the  
227 phases reducing strength of easterlies (1-4) and also phase 5, are less strongly easterly,  
228 whilst the phases increasing strength of easterlies lie roughly on the curve. To confirm  
229 this, taking the mean zonal wind of all active ( $-4.81\text{ms}^{-1}$ ), and inactive days ( $-5.02\text{ms}^{-1}$ ),  
230 and performing a one-sided t-test, it is found that the mean zonal winds of active days  
231 are less easterly, significant at the 1% level (a similar but weaker result is found using  
232 MERRA-2, significant at the 5% level). Despite this asymmetry, it is still possible that  
233 rather than the MJO influencing the zonal winds (or vice-versa), the correlation could  
234 result from a third process influencing both the MJO amplitude and zonal winds sep-  
235 arately.

236 Whilst the MJO can explain some of the inter-annual and decadal variability of the  
237 zonal winds, the fairly weak correlation and low percentage of explained change in mean  
238 suggests other factors must be involved. Figure 4 shows dry minus wet composites of geopo-  
239 tential height at 700hPa (Z700), for INTERANNUAL and DECADEAL. In both the IN-  
240 TERANNUAL and DECADEAL the 700hPa wind anomalies follow closely the gradients  
241 in anomaly in Z700, as expected. Figure 4c also shows the 850hPa temperature for DECADEAL.  
242 By the hypsometric equation, the geopotential thickness between two layers is directly  
243 proportional to the mean temperature within them, and this composite is therefore sim-  
244 ilar to the geopotential thickness between 700hPa and 925hPa (not shown).

245 In the INTERANNUAL composite (Figure 4a), there is a geopotential anomaly over  
246 the eastern Sahel, extending over Arabia. This area is also where both geopotential thick-  
247 ness and Z700 are maximal in the climatology (Figure S1c,d). Therefore, in dry years,  
248 the maxima in geopotential thickness and Z700 are increased, causing a larger merid-  
249 ional geopotential gradient from the Sahel to the Congo, consistent with increased strength  
250 of easterly winds.

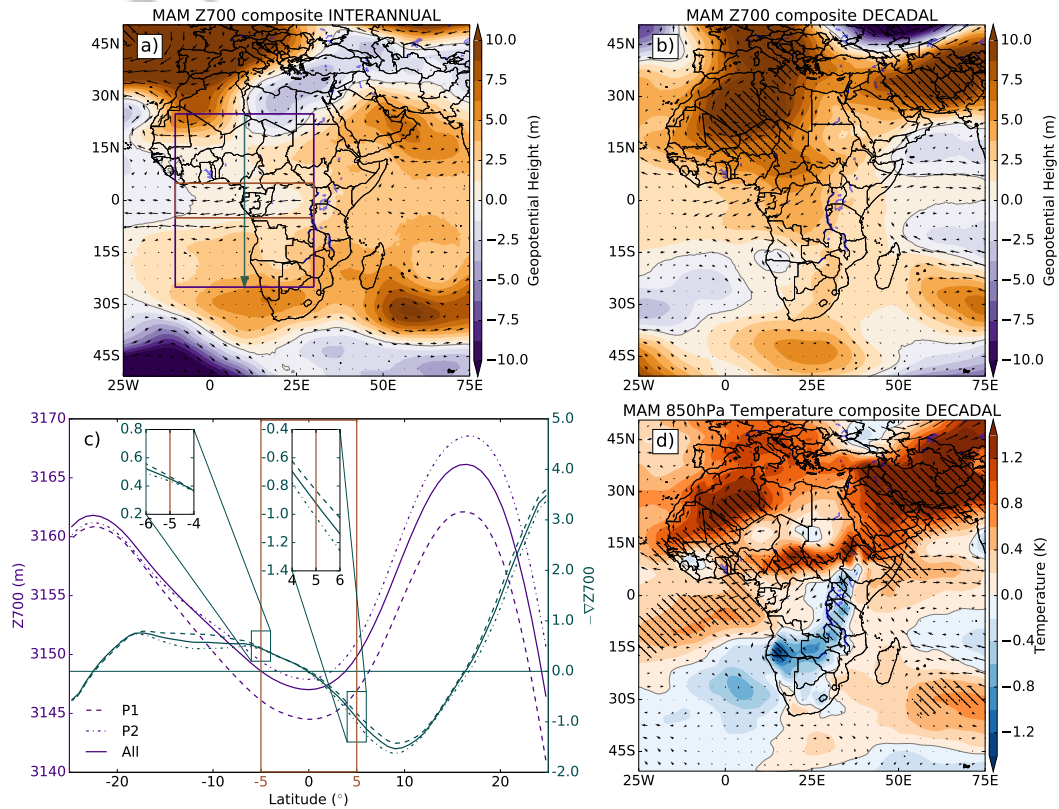


**Figure 4.** Inter-annual and decadal geopotential patterns over Africa. (a) Composites of 700hPa geopotential height and winds for (a) INTERANNUAL, and (b), DECADAL. (c) Transect of mean geopotential height (purple) across each latitude for the purple box shown in a, and gradient of the geopotential height (blue) multiplied by -1, following blue arrow shown in a, for P1 (dashed), P2 (dotted), all years (solid). Inset boxes show geopotential gradients zoomed in to edges of zonal wind box (brown box). (d) 850hPa temperature and 700hPa winds for DECADAL, hatching denotes areas where the composite values are significantly different from 0.

251 In the DECADEAL composites (Figure 4c,d), there are large similarities between  
252 the composites of Z700 and 850hPa temperature. An anomaly over the eastern Sahel,  
253 as in Figure 4a also stands out in both of these, with positive anomalies, reducing in mag-  
254 nitude from 15°N southward through the equator. This again gives an increased geopo-  
255 tential gradient at 700hPa, consistent with increased strength of easterly winds. Two large  
256 anomalies stand out over the west Sahara, and Arabian peninsula. These are the approx-  
257 imate locations of the summertime SHL and Arabian Heat Low (AHL). The 700hPa-925hPa  
258 geopotential thickness is a common measure of the strength of the SHL, as defined by  
259 Lavaysse et al. (2009), implying that both the SHL and AHL have increased in strength.

260 Figure 4c shows the latitudinally averaged Z700 across the purple box in Figure  
261 4a, and latitudinal gradient of Z700 multiplied by  $-1$  over this region, for P1, P2, and  
262 all years. An increase in Z700 across the region in P2 compared with P1 is evident. There  
263 is also a maximum (trough) in the gradient at roughly 10°N, with P2 displaying a stronger  
264 maximum. This causes a stronger gradient on the north side of the zonal wind box (5°N:  
265 right inset of Figure 4c) whilst at the southern edge of the box (5°S: left inset of Fig-  
266 ure 4c) such a pattern is absent. This shows that the increased meridional geopotential  
267 gradient across the zonal wind box is related to the increased geopotential gradient to  
268 the north, from the increasingly strong maximum in the Z700 in the eastern Sahel. This  
269 is also apparent in MERRA-2 (Figure S2d). In Figure 4d, from P1 to P2, the increase  
270 in temperature (and geopotential thickness) is driven by a more rapidly warming east-  
271 ern Sahel and west Sahara, than over the Congo basin, increasing the meridional geopo-  
272 tential gradient at 700hPa, with increasingly strong easterly winds over the Congo re-  
273 gion and drier East Africa.

274 Another possible mechanism could be analogous to equatorial superrotation (Kraucunas  
275 & Hartmann, 2005; Dima et al., 2005; Yang et al., 2013). Rainfall is associated with or-  
276 ganised convection which can excite Rossby wave propagation and convergence of zonal  
277 momentum to the source of the disturbances. Further, any regional wind change influ-  
278 ences divergence; an easterly anomaly to the west, reducing in magnitude eastwards, pro-  
279 duces a decrease in moisture flux convergence over East Africa. However this alone is  
280 not enough to imply that the zonal winds drive rainfall, as anomalous heating from rain-  
281 fall can also feed back onto local convergence and circulation.

## 4 Discussion and Conclusions

This study has investigated the relationship between 700hPa zonal winds across the Gulf of Guinea and Congo basin, and rainfall during the East African long rains. It was found that the seasonal mean 700hPa zonal wind over this area is strongly correlated with long rains rainfall totals ( $r=0.73$ ). Considering periods similar to Wainwright et al. (2019), with a wet (P1: 1979-1997), dry (P2: 1998-2011), and recovery period (P3: 2012-2018), it was found that the same relationship is seen on decadal timescales (P2–P1), showing the importance of the zonal winds to East African climate paradox drying. Meanwhile, a recovery during P3, in agreement with Wainwright et al. (2019), is seen not only in rainfall, but also in the zonal winds. The mechanism linking the zonal winds to rainfall on inter-annual timescales is found to quantitatively explain the long rains drying trend through the decreasing trend in the zonal winds.

The mechanism driving variability in the zonal winds was explored, with some contribution coming from the MJO amplitude, both on inter-annual and decadal timescales, with wind response to MJO by phase being subtly asymmetric, as seen for rainfall (Vellinga & Milton, 2018). There was a significantly weaker MJO amplitude during P2, accounting for 18% and 13% of the decline in rainfall and wind respectively. Meanwhile, another mechanism for the inter-annual and decadal variability was shown considering changes in geopotential gradients. For inter-annual variability, these lead to stronger easterlies in drier years due to higher geopotential height over the eastern Sahel, caused by increased warming here, strengthening the geopotential gradient. For decadal variability, a similar mechanism is present, but is also aligned to increased heating around Arabia and Sahara regions.

What has not been explored is the source of differing rates of warming between the Sahel and the Congo basin. During the study period, a decadal decline in rainfall over Arabia has been reported (Almazroui et al., 2012), excess heating during this period could be linked to a decadal trend in dust activity over the Arabian Peninsula (Yu et al., 2015), that is also causing a strengthening AHL (Solmon et al., 2015). Wainwright et al. (2019) linked a deepening AHL to faster progression of the tropical rain-band over East Africa during the long rains, shortening the season, and Dunning et al. (2018) links a deepening SHL under climate change to a delayed return of the rain-band southwards in boreal autumn. This motivates further investigation into variations in seasonal Hadley Cell

314 migration, and the associated impacts on zonal flow. The eastern Sahel and Arabia re-  
315 gion has experienced a rapid, almost step-like change in temperature around the end of  
316 P1 (Almazroui et al., 2012; Attada et al., 2018; C. M. Taylor et al., 2018; Hu et al., 2019).  
317 The amplified Saharan change in temperature is linked to the observed deepening of the  
318 SHL, also responsible for the partial recovery of the Sahelian drought (Evan et al., 2015).  
319 Thus the SHL plays two key roles: affecting monsoon onset/ retreat and the latitudi-  
320 nal progression of the rain band (Lavaysse et al., 2009; Dunning et al., 2018), and as shown  
321 here by affecting zonal winds across central Africa, which are important for water vapour  
322 transport and East African rainfall (Finney et al., 2019). Further strengthening of the  
323 SHL is expected under climate change (Biasutti et al., 2009; Dong & Sutton, 2015), which  
324 through the above mechanisms could lead to further drying of the long rains.

325 Based on these results, further understanding of how relative warming rates might  
326 change in the future could provide an alternative viewpoint into the future of the long  
327 rains through changes in regional dynamics (also supported by Kent et al., 2015). For  
328 example, Giannini et al. (2018) demonstrated that in the Coupled Model Intercompar-  
329 ison Project phase 5 (CMIP5; K. E. Taylor et al., 2012), a mechanism consistent with  
330 wetter years shown here is present during MAM, with moisture advected away from the  
331 Congo towards East Africa, linked to a slower overturning circulation under climate change.

332 Whilst in the long rains, sea surface temperatures (SSTs) are less well connected  
333 to rainfall totals than in the short rains, weaker, but significant, relations do exist on both  
334 inter-annual (Ogallo, 1988; Vellinga & Milton, 2018), and longer term (Williams & Funk,  
335 2011; Liebmann et al., 2014; Bahaga et al., 2019) timescales. Understanding how the pro-  
336 cesses discussed here are influenced by SSTs could determine their predictability. Given  
337 that these zonal winds are of great importance to variability within the long rains, it should  
338 be a priority to investigate whether forecast models are able to capture this relationship.  
339 This could improve seasonal forecasting and provide useful information on the poten-  
340 tial future of the long rains.

### 341 **Acknowledgments**

342 This work was supported by the Natural Environment Research Council (NERC) through  
343 an industrial CASE award with the UK Met Office (grant NE/N008227/1). Marsham  
344 and Finney were supported by the HyCRISTAL project (grant NE/M02038X/1). Birch  
345 and Marsham were supported by the UK Research and Innovation as part of the Global

346 Challenges Research Fund, grant number NE/P021077/1 (GCRF African SWIFT). Mar-  
 347 sham was also supported by the NCAS ACREW project. Scaife was supported by the  
 348 Joint DECC/Defra Met Office Hadley Centre Climate Programme (GA01101). The au-  
 349 thors would like to thank Michael Vellinga and Dave Rowell for their helpful discussions.  
 350 All data used in this study can be freely downloaded from the following locations: GPCP  
 351 data were provided by NOAA/ESRL PSD ([www.esrl.noaa.gov/psd/data/gridded/data.gpcp.html](http://www.esrl.noaa.gov/psd/data/gridded/data.gpcp.html))  
 352 ERA-Interim Reanalysis data were provided by ECMWF ([www.ecmwf.int/en/forecasts/datasets/reanalysis-](http://www.ecmwf.int/en/forecasts/datasets/reanalysis-datasets/era-interim)  
 353 [datasets/era-interim](http://www.ecmwf.int/en/forecasts/datasets/reanalysis-datasets/era-interim)). MERRA-2 was provided by the Global Modelling and Assimila-  
 354 tion Office, NASA ([gmao.gsfc.nasa.gov/reanalysis/MERRA-2/](http://gmao.gsfc.nasa.gov/reanalysis/MERRA-2/)). Daily MJO Index data  
 355 were provided by the Bureau of Meteorology, Melbourne, Australia ([www.bom.gov.au/climate/mjo](http://www.bom.gov.au/climate/mjo)).  
 356 The authors would like to thank the reviewers for their comments, which have helped  
 357 to improve the quality and clarity of the manuscript.

## 358 References

- 359 Adler, R. F., Huffman, G. J., Chang, A., Ferraro, R., Xie, P.-P., Janowiak, J., . . .  
 360 Nelkin, E. (2003). The Version-2 Global Precipitation Climatology Project  
 361 (GPCP) monthly precipitation analysis (1979-Present). *Journal of Hy-*  
 362 *drometeorology*, 4(6), 1147–1167. doi: 10.1175/1525-7541(2003)004<1147:  
 363 *TVGPCP>2.0.CO;2*
- 364 Almazroui, M., Islam, M. N., Jones, P. D., Athar, H., & Rahman, M. A. (2012).  
 365 Recent climate change in the Arabian Peninsula: Seasonal rainfall and temper-  
 366 ature climatology of Saudi Arabia for 1979-2009. *Atmospheric Research*, 111,  
 367 29–45. doi: 10.1016/j.atmosres.2012.02.013
- 368 Attada, R., Dasari, H. P., Chowdary, J. S., Yadav, R. K., Knio, O., & Hoteit, I.  
 369 (2018). Surface air temperature variability over the Arabian Peninsula and  
 370 its links to circulation patterns. *International Journal of Climatology*, 39(1),  
 371 445–464. doi: 10.1002/joc.5821
- 372 Bahaga, T. K., Fink, A. H., & Knippertz, P. (2019). Revisiting interannual to  
 373 decadal teleconnections influencing seasonal rainfall in the Greater Horn of  
 374 Africa during the 20th century. *International Journal of Climatology*, 39(5),  
 375 2765–2785. doi: 10.1002/joc.5986
- 376 Batté, L., & Déqué, M. (2011). Seasonal predictions of precipitation over  
 377 Africa using coupled ocean-atmosphere general circulation models: Skill

- 378 of the ENSEMBLES project multimodel ensemble forecasts. *Tellus, Se-*  
 379 *ries A: Dynamic Meteorology and Oceanography*, 63A(2), 283–299. doi:  
 380 10.1111/j.1600-0870.2010.00493.x
- 381 Biasutti, M., Sobel, A. H., & Camargo, S. J. (2009). The role of the Sahara low in  
 382 summertime Sahel rainfall variability and change in the CMIP3 models. *Jour-*  
 383 *nal of Climate*, 22(21), 5755–5771. doi: 10.1175/2009JCLI2969.1
- 384 Black, E., Slingo, J., & Sperber, K. R. (2003). An observational study of the  
 385 relationship between excessively strong short rains in coastal East Africa  
 386 and Indian Ocean SST. *Monthly Weather Review*, 131(1), 74–94. doi:  
 387 10.1175/1520-0493(2003)131<0074:AOSOTR>2.0.CO;2
- 388 Camberlin, P., & Philippon, N. (2002). The East African March-May rainy season:  
 389 associated atmospheric dynamics and predictability over the 1968-97 period.  
 390 *Journal of Climate*, 15(9), 1002–1019. doi: 10.1175/1520-0442(2002)015<1002:  
 391 TEAMMR>2.0.CO;2
- 392 Camberlin, P., & Wairoto, J. G. (1997). Intraseasonal wind anomalies related to wet  
 393 and dry spells during the “long” and “short” rainy seasons in Kenya. *Theoreti-*  
 394 *cal and Applied Climatology*, 58(1-2), 57–69. doi: 10.1007/BF00867432
- 395 Dee, D. P., Uppala, S. M., Simmons, A. J., Berrisford, P., Poli, P., Kobayashi, S., ...  
 396 Vitart, F. (2011). The ERA-Interim reanalysis: configuration and performance  
 397 of the data assimilation system. *Quarterly Journal of the Royal Meteorological*  
 398 *Society*, 137(656), 553–597. doi: 10.1002/qj.828
- 399 Diem, J. E., Sung, H. S., Konecky, B. L., Palace, M. W., Salerno, J., & Hartter, J.  
 400 (2019). Rainfall characteristics and trends – and the role of Congo wester-  
 401 lies – in the western Uganda transition zone of equatorial Africa from 1983  
 402 to 2017. *Journal of Geophysical Research: Atmospheres*, 124, 1–18. doi:  
 403 10.1029/2019jd031243
- 404 Dima, I. M., Wallace, J. M., & Kraucunas, I. (2005). Tropical zonal momentum bal-  
 405 ance in the NCEP reanalyses. *Journal of the Atmospheric Sciences*, 62(7 II),  
 406 2499–2513. doi: 10.1175/JAS3486.1
- 407 Dong, B., & Sutton, R. (2015). Dominant role of greenhouse-gas forcing in the re-  
 408 covery of Sahel rainfall. *Nature Climate Change*, 5(8), 757–760. doi: 10.1038/  
 409 nclimate2664
- 410 Dunning, C. M., Black, E., & Allan, R. P. (2018). Later wet seasons with more

- 411 intense rainfall over Africa under future climate change. *Journal of Climate*,  
412 31(23), 9719–9738. doi: 10.1175/JCLI-D-18-0102.1
- 413 Dutra, E., Magnusson, L., Wetterhall, F., Cloke, H. L., Balsamo, G., Boussetta, S.,  
414 & Pappenberger, F. (2013). The 2010–2011 drought in the Horn of Africa in  
415 ECMWF reanalysis and seasonal forecast products. *International Journal of*  
416 *Climatology*, 33(7), 1720–1729. doi: 10.1002/joc.3545
- 417 Evan, A. T., Flamant, C., Lavaysse, C., Kocha, C., & Saci, A. (2015). Water  
418 vapor-forced greenhouse warming over the Sahara desert and the recent re-  
419 recovery from the Sahelian drought. *Journal of Climate*, 28(1), 108–123. doi:  
420 10.1175/JCLI-D-14-00039.1
- 421 Finney, D. L., Marsham, J. H., Walker, D. P., Birch, C. E., Woodhams, B. J., Jack-  
422 son, L. S., & Hardy, S. (2019). The effect of westerlies on East African rainfall  
423 and the associated role of tropical cyclones and the Madden-Julian Oscillation.  
424 *Quarterly Journal of the Royal Meteorological Society*. doi: 10.1002/qj.3698
- 425 Funk, C. C., Dettinger, M. D., Michaelsen, J. C., Verdin, J. P., Brown, M. E., Bar-  
426 low, M., & Hoell, A. (2008). Warming of the Indian Ocean threatens eastern  
427 and southern African food security but could be mitigated by agricultural  
428 development. *Proceedings of the National Academy of Sciences*, 105(32),  
429 11081–11086. doi: 10.1073/pnas.0708196105
- 430 Funk, C. C., & Hoell, A. (2015). The leading mode of observed and CMIP5  
431 ENSO-residual sea surface temperatures and associated changes in indo-  
432 pacific climate. *Journal of Climate*, 28(11), 4309–4329. doi: 10.1175/  
433 JCLI-D-14-00334.1
- 434 Funk, C. C., Pedreros, D., Nicholson, S., Hoell, A., Korecha, D., Galu, G., ...  
435 Pomposi, C. (2019). Examining the Potential Contributions of Extreme  
436 “Western V” Sea Surface Temperatures to the 2017 March–June East African  
437 Drought. *Bulletin of the American Meteorological Society*, 100(1), S55–S60.  
438 doi: 10.1175/BAMS-D-18-0108.1
- 439 Funk, C. C., Senay, G., Asfaw, A., & Verdin, J. (2005). Recent drought tendencies  
440 in Ethiopia and equatorial-subtropical eastern Africa. *FEWS NET Special Re-*  
441 *port*.
- 442 Gelaro, R., McCarty, W., Suárez, M. J., Todling, R., Molod, A., Takacs, L., ...  
443 Zhao, B. (2017). The modern-era retrospective analysis for research and ap-

- 444 plications, version 2 (MERRA-2). *Journal of Climate*, 30(14), 5419–5454. doi:  
445 10.1175/JCLI-D-16-0758.1
- 446 Giannini, A., Lyon, B., Seager, R., & Vignaud, N. (2018). Dynamical and ther-  
447 modynamic elements of modeled climate change at the East African mar-  
448 gin of convection. *Geophysical Research Letters*, 45(2), 992–1000. doi:  
449 10.1002/2017GL075486
- 450 Hu, L., Luo, J.-J., Huang, G., & Wheeler, M. C. (2019). Synoptic features responsi-  
451 ble for heat waves in Central-Africa, a region with strong multi-decadal trend.  
452 *Journal of Climate*, 32(22), 7951–7970. doi: 10.1175/jcli-d-18-0807.1
- 453 Indeje, M., Semazzi, F. H., & Ogallo, L. J. (2000). ENSO signals in East African  
454 rainfall seasons. *International Journal of Climatology*, 20(1), 19–46. doi: 10  
455 .1002/(SICI)1097-0088(200001)20:1<19::AID-JOC449>3.0.CO;2-0
- 456 Kalnay, E., Kanamitsu, M., Kistler, R., Collins, W., Deaven, D., Gandin, L.,  
457 ... Joseph, D. (1996). The NCEP / NCAR 40-Year Reanalysis Project.  
458 *Bulletin of the American Meteorological Society*, 77(3), 437–472. doi:  
459 10.1175/1520-0477(1996)077<0437:TNYRP>2.0.CO;2
- 460 Kendall, M. G. (1975). *Rank Correlation Methods* (4th ed.). London: Charles Grif-  
461 fin.
- 462 Kent, C., Chadwick, R., & Rowell, D. P. (2015). Understanding uncertainties in fu-  
463 ture projections of seasonal tropical precipitation. *Journal of Climate*, 28(11),  
464 4390–4413. doi: 10.1175/JCLI-D-14-00613.1
- 465 Kilavi, M., MacLeod, D., Ambani, M., Robbins, J., Dankers, R., Graham, R., ...  
466 Todd, M. C. (2018). Extreme rainfall and flooding over central Kenya in-  
467 cluding Nairobi city during the long-rains season 2018: Causes, predictabil-  
468 ity, and potential for early warning and actions. *Atmosphere*, 9(12). doi:  
469 10.3390/atmos9120472
- 470 Kraucunas, I., & Hartmann, D. L. (2005). Equatorial superrotation and the  
471 factors controlling the zonal-mean zonal winds in the tropical upper tro-  
472 posphere. *Journal of the Atmospheric Sciences*, 62(2), 371–389. doi:  
473 10.1175/JAS-3365.1
- 474 Lavaysse, C., Flamant, C., Janicot, S., Parker, D. J., Lafore, J. P., Sultan, B.,  
475 & Pelon, J. (2009). Seasonal evolution of the West African heat low: A  
476 climatological perspective. *Climate Dynamics*, 33(2-3), 313–330. doi:

- 477 10.1007/s00382-009-0553-4
- 478 Liebmann, B., Hoerling, M. P., Funk, C. C., Bladé, I., Dole, R. M., Allured, D.,  
479 ... Eischeid, J. K. (2014). Understanding recent eastern Horn of Africa  
480 rainfall variability and change. *Journal of Climate*, 27(23), 8630–8645. doi:  
481 10.1175/JCLI-D-13-00714.1
- 482 Liebmann, B., & Smith, C. A. (1996). Description of a complete (interpolated) out-  
483 going longwave radiation dataset. *Bulletin of the American Meteorological So-*  
484 *ciety*, 77(6), 1275–1277.
- 485 Lyon, B. (2014). Seasonal drought in the Greater Horn of Africa and its recent  
486 increase during the March-May long rains. *Journal of Climate*, 27(21), 7953–  
487 7975. doi: 10.1175/JCLI-D-13-00459.1
- 488 Lyon, B., & Dewitt, D. G. (2012). A recent and abrupt decline in the East  
489 African long rains. *Geophysical Research Letters*, 39(2), L02702. doi:  
490 10.1029/2011GL050337
- 491 Madden, R. A., & Julian, P. R. (1971). Detection of a 40-50 day oscillation in the  
492 zonal wind in the tropical Pacific. *Journal of the Atmospheric Sciences*, 28(5),  
493 702–708. doi: 10.1175/1520-0469(1971)028<0702:DOADOI>2.0.CO;2
- 494 Madden, R. A., & Julian, P. R. (1972). Description of global-scale circulation cells  
495 in the tropics with a 40-50 day period. *Journal of the Atmospheric Sciences*,  
496 29(6), 1109–1123. doi: 10.1175/1520-0469(1972)029<1109:DOGSCC>2.0.CO;2
- 497 Maidment, R. I., Allan, R. P., & Black, E. (2015). Recent observed and simulated  
498 changes in precipitation over Africa. *Geophysical Research Letters*, 42(19), 1–  
499 10. doi: 10.1002/2015GL065765
- 500 Mann, H. B. (1945). Nonparametric tests against trend. *Econometrica*, 13(3), 245–  
501 259.
- 502 Nicholson, S. E. (2017). Climate and climatic variability of rainfall over eastern  
503 Africa. *Reviews of Geophysics*, 55(3), 590–635. doi: 10.1002/2016RG000544
- 504 Nicholson, S. E., & Entekhabi, D. (1986). The quasi-periodic behavior of rainfall  
505 variability in Africa and its relationship to the southern oscillation. *Archives*  
506 *for Meteorology, Geophysics, and Bioclimatology Series A*, 34(3-4), 311–348.  
507 doi: 10.1007/BF02257765
- 508 Nkunzimana, A., Bi, S., Jiang, T., Wu, W., & Abro, M. I. (2019). Spatiotem-  
509 poral variation of rainfall and occurrence of extreme events over Burundi

- 510 during 1960 to 2010. *Arabian Journal of Geosciences*, 12(176). doi:  
511 10.1007/s12517-019-4335-y
- 512 Ogallo, L. J. (1988). Relationships between seasonal rainfall in East Africa and the  
513 Southern Oscillation. *Journal of Climatology*, 8(1), 31–43. doi: 10.1002/joc  
514 .3370080104
- 515 Okoola, R. E. (1999a). A diagnostic study of the eastern Africa monsoon circu-  
516 lation during the northern hemisphere spring season. *International Journal of*  
517 *Climatology*, 19(2), 143–168. doi: 10.1002/(SICI)1097-0088(199902)19:2<143::  
518 AID-JOC342>3.0.CO;2-U
- 519 Okoola, R. E. (1999b). Midtropospheric Circulation Patterns Associated with Ex-  
520 treme Dry and Wet Episodes over Equatorial Eastern Africa during the North-  
521 ern Hemisphere Spring. *Journal of Applied Meteorology*, 38(8), 1161–1169. doi:  
522 10.1175/1520-0450(1999)038<1161:MCPAWE>2.0.CO;2
- 523 Otieno, V. O., & Anyah, R. O. (2013). CMIP5 simulated climate conditions of the  
524 Greater Horn of Africa (GHA). Part II: Projected climate. *Climate Dynamics*,  
525 41(7-8), 2099–2113. doi: 10.1007/s00382-013-1694-z
- 526 Pohl, B., & Camberlin, P. (2006a). Influence of the Madden-Julian Oscillation on  
527 East African rainfall. II: March-May season extremes and interannual vari-  
528 ability. *Quarterly Journal of the Royal Meteorological Society*, 132(621),  
529 2541–2558. doi: 10.1256/qj.05.223
- 530 Pohl, B., & Camberlin, P. (2006b). Influence of the Madden-Julian Oscillation  
531 on East African rainfall. I: Intraseasonal variability and regional dependency.  
532 *Quarterly Journal of the Royal Meteorological Society*, 132(621), 2521–2539.  
533 doi: 10.1256/qj.05.104
- 534 Rácz, Z., & Smith, R. K. (1999). The dynamics of heat lows. *Quarterly*  
535 *Journal of the Royal Meteorological Society*, 125(533), 225–252. doi:  
536 10.1002/qj.49712555313
- 537 Rowell, D. P., Booth, B. B., Nicholson, S. E., & Good, P. (2015). Reconciling past  
538 and future rainfall trends over East Africa. *Journal of Climate*, 28(24), 9768–  
539 9788. doi: 10.1175/JCLI-D-15-0140.1
- 540 Saji, N. H., Goswami, B. N., Vinayachandran, P. N., & Yamagata, T. (1999). A  
541 dipole mode in the tropical Indian ocean. *Nature*, 401(6751), 360–363. doi: 10  
542 .1038/43854

- 543 Shongwe, M. E., van Oldenborgh, G. J., van den Hurk, B., & van Aalst, M. (2011).  
544 Projected changes in mean and extreme precipitation in Africa under global  
545 warming. Part II: East Africa. *Journal of Climate*, *24*(14), 3718–3733. doi:  
546 10.1175/2010JCLI2883.1
- 547 Solmon, F., Nair, V. S., & Mallet, M. (2015). Increasing Arabian dust activity and  
548 the Indian summer monsoon. *Atmospheric Chemistry and Physics*, *15*(14),  
549 8051–8064. doi: 10.5194/acp-15-8051-2015
- 550 Taylor, C. M., Fink, A. H., Klein, C., Parker, D. J., Guichard, F., Harris, P. P., &  
551 Knapp, K. R. (2018). Earlier seasonal onset of intense mesoscale convective  
552 systems in the Congo basin since 1999. *Geophysical Research Letters*, *45*(24),  
553 13,458–13,467. doi: 10.1029/2018GL080516
- 554 Taylor, K. E., Stouffer, R. J., & Meehl, G. A. (2012). An overview of CMIP5 and  
555 the experiment design. *Bulletin of the American Meteorological Society*, *93*(4),  
556 485–498. doi: 10.1175/BAMS-D-11-00094.1
- 557 Vellinga, M., & Milton, S. (2018). Drivers of interannual variability of the East  
558 African ‘Long Rains’. *Quarterly Journal of the Royal Meteorological Society*.  
559 doi: 10.1002/qj.3263
- 560 Wainwright, C. M., Marsham, J. H., Keane, R. J., Rowell, D. P., Finney, D. L.,  
561 Black, E., & Allan, R. P. (2019). ‘Eastern African Paradox’ rainfall decline due  
562 to shorter not less intense Long Rains. *npj Climate and Atmospheric Science*,  
563 *2*(1), 1–9. doi: 10.1038/s41612-019-0091-7
- 564 Walker, D. P., Birch, C. E., Marsham, J. H., Scaife, A. A., Graham, R. J., & Segele,  
565 Z. T. (2019). Skill of dynamical and GHACOF consensus seasonal fore-  
566 casts of East African rainfall. *Climate Dynamics*, *53*(7), 4911–4935. doi:  
567 10.1007/s00382-019-04835-9
- 568 Wheeler, M. C., & Hendon, H. H. (2004). An all-season real-time multivariate  
569 MJO Index: Development of an index for monitoring and prediction. *Monthly*  
570 *Weather Review*, *132*(8), 1917–1932. doi: 10.1175/1520-0493(2004)132<1917:  
571 AARMMI>2.0.CO;2
- 572 Wilks, D. S. (2011). *Statistical Methods in the Atmospheric Sciences* (3rd ed.). Ox-  
573 ford: Elsevier.
- 574 Williams, A. P., & Funk, C. C. (2011). A westward extension of the warm pool leads  
575 to a westward extension of the Walker circulation, drying eastern Africa. *Cli-*

- 576 *mate Dynamics*, 37(11-12), 2417–2435. doi: 10.1007/s00382-010-0984-y
- 577 Yang, W., Seager, R., & Cane, M. A. (2013). Zonal momentum balance in the tropi-  
578 cal atmospheric circulation during the global monsoon mature months. *Journal*  
579 *of the Atmospheric Sciences*, 70(2), 583–599. doi: 10.1175/JAS-D-12-0140.1
- 580 Yang, W., Seager, R., Cane, M. A., & Lyon, B. (2014). The East African long rains  
581 in observations and models. *Journal of Climate*, 27(19), 7185–7202. doi: 10  
582 .1175/JCLI-D-13-00447.1
- 583 Yu, Y., Notaro, M., Liu, Z., Wang, F., Alkolibi, F., Fadda, E., & Bakhrjy, F.  
584 (2015). Climatic controls on the interannual to decadal variability in Saudi  
585 Arabian dust activity: Toward the development of a seasonal dust predic-  
586 tion model. *Journal of Geophysical Research*, 120(5), 1739–1758. doi:  
587 10.1002/2014JD022611